

Alternative interpretation of the sign reversal of secondary Bjerknes force acting between two pulsating gas bubbles

Masato Ida

*Collaborative Research Center of Frontier Simulation Software for Industrial Science,
Institute of Industrial Science, the University of Tokyo,
4-6-1 Komaba, Meguro-Ku, Tokyo 153-8505, Japan*

It is known that in a certain case, the secondary Bjerknes force, which is a radiation force acting between pulsating bubbles, changes, e.g., from attraction to repulsion as the bubbles approach each other. In this paper, a theoretical discussion of this phenomenon for two spherical bubbles is described. The present theory based on analysis of the transition frequencies of interacting bubbles [M. Ida, Phys. Lett. A **297**, 210 (2002)] provides an interpretation, different from previous ones (e.g., by Doinikov and Zavtrak [Phys. Fluids **7**, 1923 (1995)]), of the phenomenon. It is shown, for example, that the reversal that occurs when one bubble is smaller and another is larger than a resonance size is due to the second-highest transition frequency of the smaller bubble, which cannot be obtained using traditional natural-frequency analysis.

PACS numbers: 43.20.+g, 47.55.Bx, 47.55.Dz

I. INTRODUCTION

It is known that two gas bubbles pulsating in an acoustic field undergo an interaction force called the secondary Bjerknes force [1, 2, 3]. This force is attractive when the bubbles pulsate in-phase with each other, while it is repulsive otherwise; that is, the phase property of the bubbles plays an important role in determining the sign of the force. In a seminal paper published in 1984 [4], Zabolotskaya, using a linear coupled oscillator model, showed theoretically that in a certain case, the sign of the force may change as the bubbles come closer to one another. This theoretical prediction was ensured by recent experiments that captured the stable, periodic translational motion of two coupled bubbles [5], resulting from the sign reversal of the force at a certain distance between the bubbles. Zabolotskaya assumed that this sign reversal is due to variation in the natural frequencies of the interacting bubbles, which results in shifts of their pulsation phases. The theoretical formula Zabolotskaya derived to evaluate the natural frequencies of two interacting bubbles, which corresponds to one given previously by Shima [6], is represented as

$$(\omega_{10}^2 - \omega^2)(\omega_{20}^2 - \omega^2) - \frac{R_{10}R_{20}}{D^2}\omega^4 \approx 0, \quad (1)$$

where R_{10} and R_{20} are the equilibrium radii of the bubbles, ω_{10} and ω_{20} are their partial natural (angular) frequencies, ω is the angular frequency of an external sound, and D is the distance between the centers of the bubbles. This equation predicts the existence of two natural frequencies per bubble, and is symmetric; namely, it exchanges 10 and 20 in the subscripts of the variables to reproduce the same equation, meaning that the two bubbles have the same natural frequencies.

During the last decade, a number of studies regarding the sign reversal of the force have been performed [5, 7, 8, 9, 10, 11, 12, 13, 14]. Among them, Refs. [9, 10, 13] also considered the relevance of the change in

the natural frequencies (or resonance frequencies [15]) to the sign reversal. In the present paper, we focus our attention on this case, although it has been shown that other factors, such as the nonlinearity in bubble pulsation [7, 11, 12, 13, 14] and the higher-order terms appearing in the time-averaged interaction force [5] which has been neglected in previous works, can also cause the sign reversal.

In 1995, Doinikov and Zavtrak [9], using a linear mathematical model in which the multiple scattering of sound between bubbles is taken into account more rigorously, predicted again the sign reversal. They also asserted that this reversal is due to the change in the natural frequencies. They assumed that the natural frequencies of both bubbles increase as the bubbles approach each other, resulting sometimes in the sign reversal. When, for example, both bubbles are larger than the resonance size (i.e., the case of $\omega_{10} < \omega$ and $\omega_{20} < \omega$) and the distance between them is large enough, they pulsate in-phase with each other. As the bubbles approach each other, the natural frequency of a smaller bubble may first, at a certain distance, rise above the driving frequency, and in turn the bubbles' pulsations become antiphase; the force then changes from attractive to repulsive. When, on the other hand, one bubble is larger and the other is smaller than the resonance size (e.g., $\omega_{10} > \omega > \omega_{20}$) and the distance between them is large, they pulsate out-of-phase with each other and the force is repulsive. As the distance between the bubbles becomes smaller, the natural frequencies of both bubbles may rise, and when the natural frequency of a larger bubble rises above the driving frequency, the repulsive force may turn into attraction. This interpretation is supported even in more recent papers [12, 14].

Although this interpretation seems to explain the sign reversal well, it is opposed to the prediction given by Eq. (1) which reveals that the higher natural frequency (converging to the partial natural frequency of a smaller bubble for $D \rightarrow \infty$ [6, 16]) increases but the lower one

(converging to the partial natural frequency of a larger bubble for $D \rightarrow \infty$) decreases as the bubbles approach each other.

In 2001, Harkin *et al.* [13] performed an extensive theoretical study concerning the translational motion of two acoustically coupled gas bubbles in a weak and a moderate driving sound field. Their theoretical model derived from first principles supports the experimental results by Barbat *et al.* [5]. In Sec. 7 of that paper, Harkin *et al.* also considered the influence of the change in natural frequencies on the sign of the force in order to explain the sign reversal for $\omega_{10} < \omega$ and $\omega_{20} < \omega$. Their explanation based on a formula given directly by Eq. (1) is essentially the same as those by Zabolotskaya [4] and by Doinikov & Zavtrak [9, 10].

The authors should note here that all the previous theoretical models mentioned above can *describe* (or *explain*) the sign reversal. However, the *interpretation* we will provide in the present paper is different from the previous ones.

The aim of this paper is to give an alternative interpretation of the sign reversal, one that may be more accurate than the previous ones that are based on the natural-frequency analysis. Recently, having reexamined the linear coupled oscillator model used frequently to analyze the dynamics of acoustically coupled bubbles (see Ref. [16] and references therein), we found that a bubble interacting with a neighboring bubble has three “transition frequencies”, defined as *the driving frequencies for which the phase difference between an external sound and the bubble’s pulsation becomes $\pi/2$ (or $3\pi/2$)*, two of which correspond to the natural frequencies [16]. Among the three transition frequencies, the lowest one decreases and the remaining two increase as the bubbles approach each other. Meanwhile, for $D \rightarrow \infty$ only one of them converges to the partial natural frequency of the corresponding bubble. Namely, the transition frequencies defined as above are asymmetric. The use of the transition frequencies would allow us an accurate understanding of the sign reversal, because observing these frequencies provides more detailed insights of the bubbles’ phase properties rather than that provided by the natural-frequency analysis. Using the theory for the transition frequencies, we arrive at a novel interpretation of the sign reversal.

II. THEORIES

In this section, we briefly review the previously expounded theories regarding the natural frequencies, the transition frequencies, and the secondary Bjerknes force.

A. Natural frequencies and transition frequencies

Let us consider the linear volume oscillation of N -bubble system immersed in an incompressible liquid. Suppose that the time-dependent radius of bubble j , R_j ,

can be represented as $R_j = R_{j0} + e_j(t)$ and $|e_j| \ll R_{j0}$, where R_{j0} and e_j are the equilibrium radius and the deviation of the radius, respectively, and $j = 1, 2, \dots, N$. The radius deviation can be determined by solving the linear oscillator model (see, e.g., Ref. [17]),

$$\ddot{e}_j + \omega_{j0}^2 e_j + \delta_j \dot{e}_j = -\frac{p_{d,j}}{\rho R_{j0}}, \quad (2)$$

where

$$\omega_{j0} = \sqrt{\frac{3\kappa_j P_0 + (3\kappa_j - 1)2\sigma/R_{j0}}{\rho R_{j0}^2}}$$

are the partial natural (angular) frequencies of bubble j , δ_j is the damping coefficient determined based on the damping characteristics of the bubbles [18], $p_{d,j}$ is the driving pressure acting on bubble j , κ_j is the effective polytropic exponent of the gas inside the bubbles, P_0 is the static pressure, σ is the surface tension, ρ is the density of the liquid surrounding the bubbles, and the over-dots denote the time derivation. The driving pressure is represented by the sum of p_{ex} and the sound pressure scattered by the surrounding bubbles, p_s , as

$$p_{d,j} = p_{\text{ex}} + \sum_{k=1, k \neq j}^N p_{s,jk}.$$

The value of $p_{s,jk}$ is determined by integrating the momentum equation for linear sound waves, $\partial p / \partial r = -\rho \partial u / \partial t$, coupled with the divergence-free condition, $\partial(r^2 u) / \partial r = 0$, where r is the radial coordinate measured from the center of a bubble and u is the velocity along r . Resultantly, the driving pressure is determined as

$$p_{d,j} = p_{\text{ex}} + \rho \sum_{k=1, k \neq j}^N \frac{R_{k0}^2}{D_{jk}} \ddot{e}_k, \quad (3)$$

where D_{jk} is the distance between the centers of bubbles j and k .

In a single-bubble case (i.e., for $N = 1$), Eq. (2) is reduced to

$$\ddot{e}_1 + \omega_{10}^2 e_1 + \delta_1 \dot{e}_1 = -\frac{p_{\text{ex}}}{\rho R_{10}}. \quad (4)$$

Assuming that p_{ex} is written in the form of $p_{\text{ex}} = -P_a \sin \omega t$ (P_a is a positive constant), the harmonic steady-state solution of Eq. (4) is given by

$$e_1 = K_{S1} \sin(\omega t - \phi_{S1}),$$

with

$$K_{S1} = \frac{P_a}{\rho_0 R_{10}} \sqrt{\frac{1}{(\omega_{10}^2 - \omega^2)^2 + \delta_1^2 \omega^2}},$$

$$\phi_{S1} = \tan^{-1} \left(\frac{\delta_1 \omega}{\omega_{10}^2 - \omega^2} \right).$$

From this result, one knows that the phase difference of $\phi_{S1} = \pi/2$ appears (or, roughly speaking, the phase reversal takes place) only at the natural frequency ω_{10} [19], and the resonance response occurs at (or, more correctly, near) the same driving frequency.

For $N = 2$, Eq. (2) is reduced to

$$\ddot{e}_1 + \omega_{10}^2 e_1 + \delta_1 \dot{e}_1 = -\frac{p_{\text{ex}}}{\rho R_{10}} - \frac{R_{20}^2}{R_{10} D} \ddot{e}_2, \quad (5)$$

$$\ddot{e}_2 + \omega_{20}^2 e_2 + \delta_2 \dot{e}_2 = -\frac{p_{\text{ex}}}{\rho R_{20}} - \frac{R_{10}^2}{R_{20} D} \ddot{e}_1, \quad (6)$$

where $D = D_{12} = D_{21}$. It is known that for a weak forcing (i.e., $P_a \ll P_0$), this system has third-order accuracy with respect to $1/D$, although it has terms of up to first order (the last terms) [13]. The harmonic steady-state solution for e_1 is

$$e_1 = K_1 \sin(\omega t - \phi_1),$$

where

$$K_1 = \frac{P_a}{R_{10} \rho} \sqrt{A_1^2 + B_1^2},$$

$$\phi_1 = \tan^{-1} \left(\frac{B_1}{A_1} \right) \in [0, 2\pi],$$

with

$$A_1 = \frac{H_1 F + M_2 G}{F^2 + G^2}, \quad B_1 = \frac{H_1 G - M_2 F}{F^2 + G^2},$$

$$F = L_1 L_2 - \frac{R_{10} R_{20}}{D^2} \omega^4 - M_1 M_2,$$

$$G = L_1 M_2 + L_2 M_1, \quad H_1 = L_2 + \frac{R_{20}}{D} \omega^2,$$

$$L_1 = \omega_{10}^2 - \omega^2, \quad L_2 = \omega_{20}^2 - \omega^2,$$

$$M_1 = \delta_1 \omega, \quad M_2 = \delta_2 \omega.$$

Exchanging 1 and 2 (or 10 and 20) in the subscripts of these equations yields the expressions for bubble 2.

The formula for the natural frequency, Eq. (1), is derived so that $K_1 \rightarrow \infty$ for $\delta_1 \rightarrow 0$ and $\delta_2 \rightarrow 0$. Namely,

$$F = L_1 L_2 - \frac{R_{10} R_{20}}{D^2} \omega^4 = 0.$$

As mentioned already, this equation predicts the existence of up to two natural frequencies in a double-bubble system.

The transition frequencies of bubble 1 are determined so that ϕ_1 becomes $\pi/2$ (or $3\pi/2$). Because $F^2 + G^2 \neq 0$ [16], the resulting formula for deriving the transition frequencies of bubble 1 is

$$H_1 F + M_2 G = 0. \quad (7)$$

Assuming $\delta_1 \rightarrow 0$ and $\delta_2 \rightarrow 0$ reduces this to

$$H_1 F = \left(L_2 + \frac{R_{20}}{D} \omega^2 \right) \left(L_1 L_2 - \frac{R_{10} R_{20}}{D^2} \omega^4 \right) = 0. \quad (8)$$

As was proven in Ref. [16], this equation predicts the existence of up to three transition frequencies per bubble. Furthermore, as pointed out in the same article, the terms in the second (\dots) of Eq. (8) are the same as those on the left-hand side of Eq. (1). These results mean that in a double-bubble case the phase reversal of a bubble's pulsation can take place not only at its natural frequencies but also at one other frequency. Because $H_1 \neq H_2$, Eq. (8) (and also Eq. (7)) is asymmetric, meaning that the bubbles have different transition frequencies.

A preliminary discussion for a N -bubble system [20] showed that a bubble in the system has up to $2N - 1$ transition frequencies, N ones of which correspond to the natural frequency. Namely, a bubble has an odd number of transition frequencies. This result can be understood as follows: Even in a multibubble case, a bubble's pulsation may be in-phase or out-of-phase with a driving sound [21] when the driving frequency is much lower or much higher, respectively, than its natural frequencies; thus, in order to interpolate these two extremes consistently an odd number of phase reversals are necessary [20].

B. Secondary Bjerknes force

The secondary Bjerknes force acting between the bubbles for sufficiently weak forcing is expressed with [1, 2, 3, 4, 5, 13]

$$\mathbf{F} \propto \langle \dot{V}_1 \dot{V}_2 \rangle \frac{\mathbf{r}_2 - \mathbf{r}_1}{\|\mathbf{r}_2 - \mathbf{r}_1\|^3} \propto K_1 K_2 \cos(\phi_1 - \phi_2) \frac{\mathbf{r}_2 - \mathbf{r}_1}{\|\mathbf{r}_2 - \mathbf{r}_1\|^3}, \quad (9)$$

where V_j and \mathbf{r}_j are the volume and the position, respectively, of bubble j , $\langle \dots \rangle$ denotes the time average, and $\|\mathbf{r}_2 - \mathbf{r}_1\| = D$. The sign reversal of this force occurs only when the sign of $\cos(\phi_1 - \phi_2)$ (or of $\langle \dot{V}_1 \dot{V}_2 \rangle$) changes, because $K_1 > 0$ and $K_2 > 0$. If the phase shifts resulting from the radiative interaction between bubbles are neglected, this force is repulsive when ω stays between ω_{10} and ω_{20} , and is attractive otherwise [1]. In the case where the radiative interaction is taken into consideration, the frequency within which the force is repulsive shifts toward a higher range, see, e.g., Refs. [9, 10].

The formulae reviewed above, except for that regarding the transition frequencies (Eqs. (7) and (8)), are classical, and almost the same ones have previously been used in Ref. [4]. As will be shown in the next section, however, the following investigation based on Eq. (7) coupled with Eq. (9) gives a different interpretation of the sign reversal from the previous ones described using only the natural frequencies.

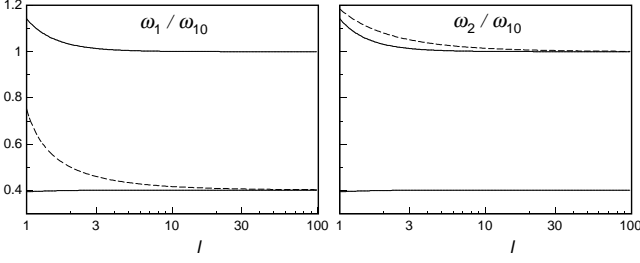


FIG. 1: Transition frequencies ω_1 (rad/s) and ω_2 (rad/s) for $R_{10} = 2$ mm, $R_{20} = 5$ mm, and the reduced damping, normalized by ω_{10} (rad/s). The dashed lines show the transition frequencies that do not cause the resonance.

III. RESULTS AND DISCUSSION

In this section, we investigate the relationship between the transition frequencies and the sign of the secondary Bjerknes force by using some examples. The first example is the case of $R_{10} = 2$ mm and $R_{20} = 5$ mm, which corresponds to a case used in Ref. [10]. We assume that the bubbles are filled with a gas having a specific heat ratio of $\gamma = 1.4$, and the surrounding material is water ($\sigma = 0.0728$ N/m, $\rho = 1000$ kg/m³, $P_0 = 1$ atm, and the speed of sound $c = 1500$ m/s). For the damping coefficient, we adopt that used for radiation and thermal losses:

$$\delta_j = \frac{\omega^2 R_{j0}}{c} + \beta_{th,j}, \quad (10)$$

where the thermal damping coefficient $\beta_{th,j}$ and the effective polytropic exponent κ_j are determined by [9, 18, 22]

$$\beta_{th,j} = \frac{\omega_{j0}^2}{\omega} d_{th,j},$$

$$\kappa_j = \gamma \left[\left(1 + d_{th,j}^2 \right) \left(1 + \frac{3(\gamma - 1)(\sinh X - \sin X)}{X(\cosh X - \cos X)} \right) \right]^{-1},$$

with

$$d_{th,j} = 3(\gamma - 1) \frac{X(\sinh X + \sin X) - 2(\cosh X - \cos X)}{X^2(\cosh X - \cos X) + 3(\gamma - 1)X(\sinh X - \sin X)},$$

$$X = R_{j0}(2\omega/\chi_G)^{1/2},$$

where we set $\chi_G = 2 \times 10^{-5}$ m² s⁻¹.

In order to clarify the following discussion, we first present results for the idealized condition of $\delta_j \approx 0$ by resetting $\delta_j \rightarrow \delta_j/100$, and subsequently provide results given by the direct use of Eq. (10). Figure 1 shows the transition frequencies of the bubbles, ω_1 and ω_2 , calculated using Eq. (7) with the reduced damping, normalized by ω_{10} ($= \omega_1$ for $D \rightarrow \infty$). In those figures, l denotes the normalized distance defined as $l = D/(R_{10} + R_{20})$. As mentioned previously, we can observe three transition

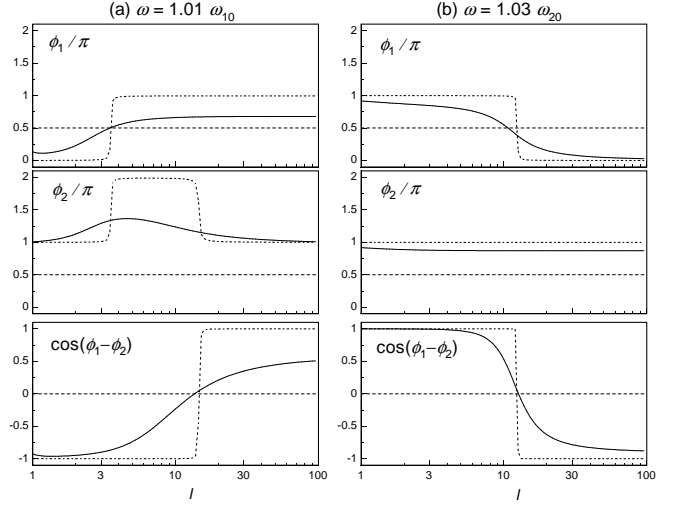


FIG. 2: ϕ_1/π , ϕ_2/π , and $\cos(\phi_1 - \phi_2)$ for (a) $\omega = 1.01\omega_{10}$ (rad/s) and (b) $\omega = 1.03\omega_{20}$ (rad/s), as functions of l . The dashed curves and the solid lines show the results given using the reduced damping and the real damping, respectively.

frequencies, only one of which converges to ω_{j0} of the corresponding bubble for $l \rightarrow \infty$. The second-highest transition frequency of bubble 2 is almost equal to the highest one of bubble 1; thus, the highest one of bubble 2 is higher than that of bubble 1. The second highest one of bubble 1 and the highest one of bubble 2 do not cause the resonance response [16].

The dashed curves displayed in Fig. 2(a) show ϕ_1 , ϕ_2 , and $\cos(\phi_1 - \phi_2)$, respectively, as functions of l . Here the driving frequency is assumed to be $\omega = 1.01\omega_{10}$, i.e., slightly above ω_{10} . (In the present study, the driving frequency is set as $\omega \approx \omega_{10}$ or $\omega \approx \omega_{20}$ so that the sign reversal takes place at a sufficiently large l where the accuracy of Eqs. (5) and (6) is guaranteed.) As mentioned in Sec. I, it is known already that the sign reversal can take place when $\omega > \omega_{10} > \omega_{20}$ or $\omega_{10} > \omega > \omega_{20}$; the present setting corresponds to the former case. We can observe one and two sharp shifts of ϕ_1 and ϕ_2 , respectively. At $l \approx 3$, both ϕ_1 and ϕ_2 shift almost simultaneously, but the sign reversal does not occur because the phase difference $\phi_1 - \phi_2$ is hardly changed. At $l \approx 13$, only ϕ_2 shifts, resulting in the sign reversal. In the former case, the phase shifts are caused by the natural frequencies. As mentioned previously, when $\delta_j \approx 0$ both the bubbles have (almost) the same natural frequencies. The simultaneous phase shift, thus, appears. The change of ϕ_2 in the later case is apparently due to the highest transition frequency of bubble 2, which cannot be obtained by the traditional natural-frequency analysis. Namely, this sign reversal cannot be interpreted by using only the natural frequencies.

We should note here that, to compute the phase delays ϕ_1 and ϕ_2 , we used the “atan2(a, b)” function in the C language, which returns $\tan^{-1}(b/a) \in [-\pi, \pi]$, and, fur-

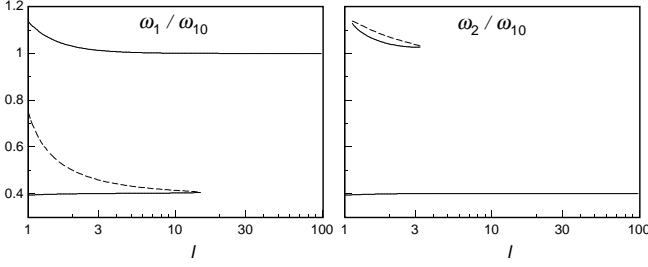


FIG. 3: Same as in Fig. 1, but for the real damping.

thermore, adopted the operation

$$\phi_j = \begin{cases} \text{atan2}(A_j, B_j) + 2\pi & \text{if } \text{atan2}(A_j, B_j) < 0, \\ \text{atan2}(A_j, B_j) & \text{otherwise} \end{cases}$$

in order to obtain results for $l \gg 1$ that are consistent with the established knowledge of single-bubble dynamics, e.g., $\phi_j \approx \pi$ when $\omega > \omega_{j0}$ and $\delta_j \approx 0$ ($j = 1$ or 2).

The dashed curves displayed in Fig. 2(b) show results for $\omega = 1.03\omega_{20}$ ($= 0.413\omega_{10}$), i.e., for $\omega_{10} > \omega > \omega_{20}$. In this case, we can observe only one sharp shift of ϕ_1 at $l \approx 12$, causing the sign reversal. This shift of ϕ_1 is due to the second-highest transition frequency of bubble 1 (this frequency also not corresponding to the natural frequency!), because the lowest transition frequencies of both the bubbles decrease as l decreases.

These results reveal that in the above cases, the transition frequencies other than the natural frequencies cause the sign reversal of the secondary Bjerknes force. This conclusion is obviously different from the previous interpretations described by means of the natural frequencies [4, 9, 10, 13].

It is interesting to point out that, in the case where $\omega > \omega_{10} > \omega_{20}$ and $\omega \approx \omega_{10}$, the phase delay of the larger bubble was sometimes greater than π (see Fig. 2(a)). Such a result cannot be given by a single-bubble model which predicts a phase delay of up to π . This may be explained as follows: When $\omega > \omega_{10} > \omega_{20}$ is true and l is sufficiently large, both bubbles pulsate out-of-phase with p_{ex} , emitting sound waves whose phases are also out-of-phase with p_{ex} . As l decreases, if $\omega \approx \omega_{10}$, the amplitude of the sound wave emitted by bubble 1 measured at \mathbf{r}_2 can be greater than the amplitude of p_{ex} . In this situation, bubble 2 is driven by a sound wave whose oscillation phase is delayed by almost π from that of p_{ex} . This results in $\phi_2 > \pi$, because the pulsation phase of bubble 2 delays further from that of the sound wave.

We show the here results given by using Eq. (10) in order to examine the influences of the damping effects on the sign reversal and phase shifts. Figure 3 shows the recalculated transition frequencies. As already discussed [16], when the damping effects are not negligible, the bubbles have only one transition frequency in the large- l region. The solid curves displayed in Fig. 2 show ϕ_1 ,

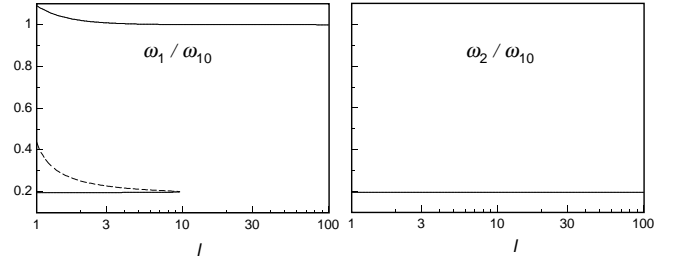


FIG. 4: Transition frequencies ω_1 (rad/s) and ω_2 (rad/s) for $R_{10} = 1 \mu\text{m}$, $R_{20} = 4 \mu\text{m}$, and the real damping, normalized by ω_{10} (rad/s).

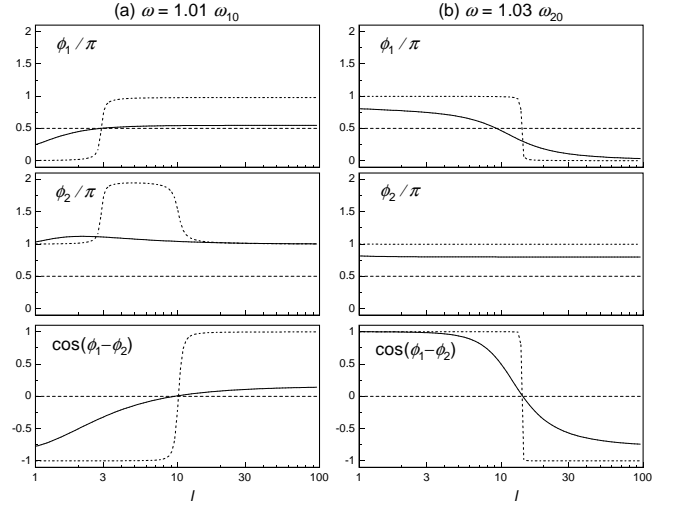


FIG. 5: ϕ_1/π , ϕ_2/π , and $\cos(\phi_1 - \phi_2)$ for (a) $\omega = 1.01\omega_{10}$ (rad/s) and (b) $\omega = 1.03\omega_{20}$ (rad/s). The dashed curves denote the results for the reduced damping.

ϕ_2 , and $\cos(\phi_1 - \phi_2)$ for $\omega = 1.01\omega_{10}$ and $\omega = 1.03\omega_{20}$. Their tendencies are similar to those given with the reduced damping, although their profiles are smoothed significantly (Such a smoothing of the phase change by the damping effects is well known for a single-bubble case) and the points at which the sign reversal takes place are shifted slightly; the positions of these points are, in the case of $\omega = 1.01\omega_{10}$, $l \approx 13.59$ for δ_j and $l \approx 14.57$ for $\delta_j/100$, and, in the case of $\omega = 1.03\omega_{20}$, $l \approx 12.66$ for δ_j and $l \approx 12.48$ for $\delta_j/100$. Moreover, ϕ_2 for $\omega = 1.01\omega_{10}$ does not exceed $3\pi/2$ (the minimum value of ω_2 larger than ω_{10} is $1.027\omega_{10}$.); even so, the sign reversal occurs at almost the same point as that given with $\delta_j/100$, away from the point where $\phi_1 = \pi/2$. This result may be interpreted as the “vestige” of the highest transition frequency of the larger bubble having given rise to this sign reversal. Detailed theoretical discussions for the slight shift in l for $\cos(\phi_1 - \phi_2) = 0$ due to the damping effects will be provided in a future paper.

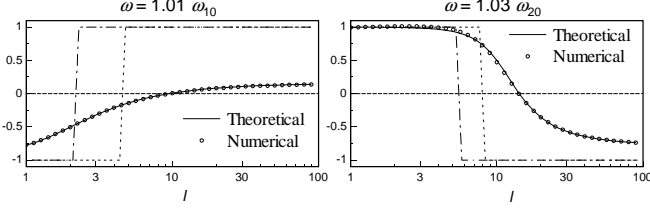


FIG. 6: Comparison between the theoretical and the numerical results. The lines and the circles denote the theoretical and the numerical results, respectively, of $\cos(\phi_1 - \phi_2)$ for $\omega = 1.01\omega_{10}$ (rad/s) and $1.03\omega_{20}$ (rad/s). Additionally, $\text{sgn}(\langle \dot{V}_1 \dot{V}_2 \rangle)$ for $P_a/P_0 = 0.2$ (the dots) and 0.5 (the dash-dotted curves) are plotted for a brief investigation of nonlinear effects.

Next, we show results for smaller bubbles ($R_{10} = 1 \mu\text{m}$ and $R_{20} = 4 \mu\text{m}$). The value for viscous loss is used for the damping coefficients, i.e.,

$$\delta_j = \frac{4\mu}{\rho R_{j0}^2}, \quad (11)$$

where the viscosity of water $\mu = 1.002 \times 10^{-3} \text{ kg/(m s)}$. Because the thermal effect is neglected, $\kappa = \gamma = 1.4$. Figure 4 shows the transition frequencies, and Figure 5 shows ϕ_1 , ϕ_2 , and $\cos(\phi_1 - \phi_2)$ for $\omega = 1.01\omega_{10}$ and $\omega = 1.03\omega_{20}$ ($= 0.201\omega_{10}$) with $\delta_j/100$ (the dashed curves) and δ_j (the solid curves). The qualitative natures of these results are quite similar with the previous ones; thus, additional discussion may not be necessary. Using this example, we perform here a comparative study of the theoretical results with the numerical results in order to confirm the former's correctness. In the numerical experiment, we employ the coupled RPNNP (Rayleigh, Plesset, Noltingk, Neppiras, and Poritsky) equations (see, e.g., Ref. [16]);

$$\begin{aligned} R_1 \ddot{R}_1 + \frac{3}{2} \dot{R}_1^2 - \frac{1}{\rho} p_{w,1} &= -\frac{1}{\rho} \left[p_{\text{ex}} + \frac{\rho}{D} \frac{d}{dt} (R_2^2 \dot{R}_2) \right], \\ R_2 \ddot{R}_2 + \frac{3}{2} \dot{R}_2^2 - \frac{1}{\rho} p_{w,2} &= -\frac{1}{\rho} \left[p_{\text{ex}} + \frac{\rho}{D} \frac{d}{dt} (R_1^2 \dot{R}_1) \right], \end{aligned}$$

where

$$p_{w,j} = \left(P_0 + \frac{2\sigma}{R_{j0}} \right) \left(\frac{R_{j0}}{R_j} \right)^{3\kappa} - \frac{2\sigma}{R_j} - \frac{4\mu \dot{R}_j}{R_j} - P_0.$$

This system of nonlinear differential equations are solved numerically through the use of the fourth-order Runge-Kutta method in which R_1 , R_2 , \dot{R}_1 , and \dot{R}_2 are used as dependent variables, and $\langle R_1^2 \dot{R}_1 R_2^2 \dot{R}_2 \rangle [\propto \langle \dot{V}_1 \dot{V}_2 \rangle]$ in Eq. (9)] is then calculated. The time average is performed during a sufficiently large period after the transients have decayed. Normalizing $\langle R_1^2 \dot{R}_1 R_2^2 \dot{R}_2 \rangle$ by $R_{10}^2 R_{20}^2 \max(|R_1(t) - R_{10}|) \max(|R_2(t) - R_{20}|) \omega^2 / 2$

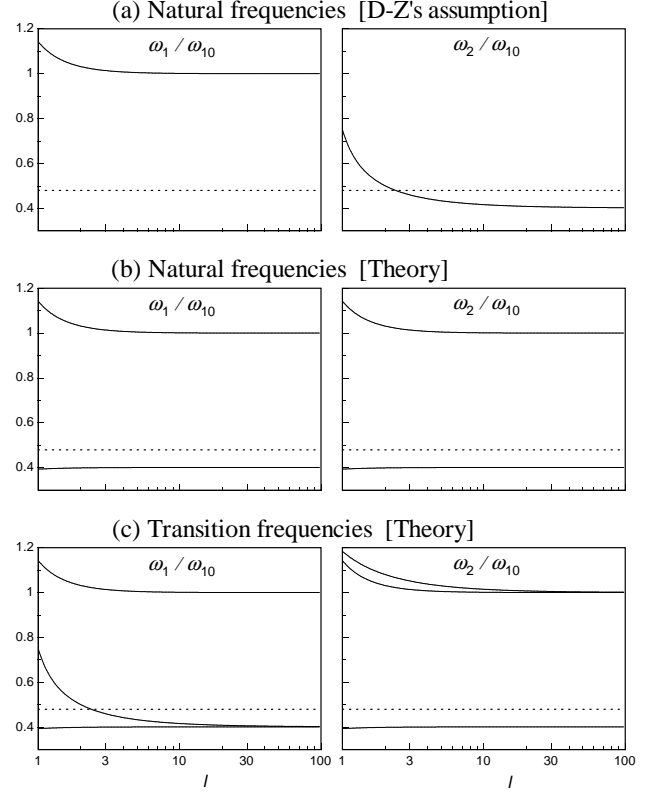


FIG. 7: Characteristic frequencies of two coupled bubbles and different interpretations of the sign reversal. The dashed lines show a typical driving frequency lying between ω_{10} and ω_{20} , where $\omega_{10} > \omega_{20}$ is assumed. Doinikov and Zavtrak assumed that the natural frequencies of both the bubbles increase as the bubbles approach each other (a). Assuming this, the sign reversal for $\omega_{10} > \omega > \omega_{20}$ seems to be explained. This assumption is, however, inconsistent with the classical theory for natural frequencies (b). The present theory can explain this reversal without such an inconsistency (c).

yields the numerical approximation of $\cos(\phi_1 - \phi_2)$, where $\max(|R_j(t) - R_{j0}|)$ indicates the pulsation amplitude of bubble j given numerically. The amplitude of the external sound is set to $P_a = 0.01P_0$. In Figure 6, the numerical and the theoretical results are displayed in piles. These results are in excellent agreement, confirming the correctness of the theoretical results given above. In the same figure, we have shown additionally $\text{sgn}(\langle \dot{V}_1 \dot{V}_2 \rangle)$ for $P_a = 0.2P_0$ (the dots) and $0.5P_0$ (the dash-dotted curves) in order to briefly investigate nonlinear effects on the sign reversal, where $\text{sgn}(X) = 1$ for $X > 0$ and $\text{sgn}(X) = -1$ otherwise. In plotting these results, we omitted the data in the case where $R_1(t) + R_2(t) > D$ was observed during the computation. As is clearly shown, increasing the driving pressure reduces the distance for which the sign reversal takes place. This result appears to be consistent with the well-known nonlinear phenomenon that a strong driving pressure

decreases a bubble's (effective) resonance frequency, see, e.g., Refs. [2, 3]. (Imagine that the transition frequencies shown, e.g., in Fig. 1 decrease but the driving frequency holds, which might shorten the distance for $\mathbf{F} = 0$.) More detailed and concrete discussions on the nonlinear effects will be provided in a future paper.

To summarize our discussion, we compare the present interpretation with the previous ones. Figure 7(a) shows the dependency of natural frequencies on l that Doinikov and Zavtrak assumed [9, 10]. Their assumption explains the sign reversal occurring when $\omega_{10} > \omega > \omega_{20}$, for example, as taking place around l at which $\omega_2 = \omega$ is true. Yet, as mentioned, their assumption is inconsistent with the theoretical results regarding natural frequencies given previously [4, 6] (see Fig. 7(b)). On the other hand, it is difficult to determine by only observing the natural frequencies that the sign reversal can take place for $\omega_{10} > \omega > \omega_{20}$, because the classical theory does not show that a kind of characteristic frequency exists in the frequency region between ω_{10} and ω_{20} . The present theory explains the sign reversal in this case as taking place around l at which $\omega_1 = \omega$ is true (see Fig. 7(c), where we assume for simplicity that the damping effect is negligible), and is consistent with the theory for natural frequencies because the transition frequencies include the natural frequencies.

IV. CONCLUSION

We have investigated the influences of change in the transition frequencies of gas bubbles, resulting from their radiative interaction, on the sign of the secondary Bjerknes force. The most important point suggested in this paper is that the transition frequencies that cannot be derived by the natural-frequency analysis cause the sign

reversal in the cases of both $\omega > \omega_{10} > \omega_{20}$ and $\omega_{10} > \omega > \omega_{20}$. This interpretation has not been proposed previously. The present results also show that the theory given in Ref. [16] for evaluating the transition frequencies of interacting bubbles is a reasonable tool for accurately understanding the mechanism of this reversal. In a paper currently in preparation [23], we will use the direct numerical simulation technique [24, 25] to verify the present theoretical results.

Lastly, we make further remarks regarding the results described in Ref. [10]. In that paper, the frequency of the external sound ($f = \omega/2\pi$) was assumed to be $f = 63$ kHz, which is 60 times higher than the partial resonance frequency of a bubble of $R_0 = 3$ mm (1.094 kHz); nevertheless, the reversal was observed at a very small l . (In Ref. [9], the driving frequency is assumed to be comparable to the partial natural frequencies of bubbles, and the bubble radii are several tens of micrometers.) This result reveals implicitly that the mathematical model proposed in Ref. [9], which takes into account the shape deviation of the bubbles, predicts such a strong increase of the transition frequencies of closely coupled large bubbles that this increase cannot be explained by the classical model for coupled oscillators used here. Derivation of the transition frequencies of Doinikov and Zavtrak's model would be an interesting subject for future study.

Acknowledgments

This work was supported by the Ministry of Education, Culture, Sports, Science, and Technology of Japan (Monbu-Kagaku-Sho) under an IT research program "Frontier Simulation Software for Industrial Science."

-
- [1] L. A. Crum, J. Acoust. Soc. Am. **57**, 1363 (1975).
 - [2] A. Prosperetti, Ultrasonics **22**, 115 (1984).
 - [3] W. Lauterborn, T. Kurz, R. Mettin, and C. D. Ohl, Adv. Chem. Phys. **110**, 295 (1999).
 - [4] E. A. Zabolotskaya, Sov. Phys. Acoust. **30**, 365 (1984).
 - [5] T. Barbat, N. Ashgriz, and C.-S. Liu, J. Fluid Mech. **389**, 137 (1999).
 - [6] A. Shima, Trans. ASME, J. Basic Eng. **93**, 426 (1971).
 - [7] H. Oguz and A. Prosperetti, J. Fluid Mech. **218**, 143 (1990).
 - [8] N. A. Pelekasis and J. A. Tsamopoulos, J. Fluid Mech. **254**, 501 (1993).
 - [9] A. A. Doinikov and S. T. Zavtrak, Phys. Fluids **7**, 1923 (1995).
 - [10] A. A. Doinikov and S. T. Zavtrak, J. Acoust. Soc. Am. **99**, 3849 (1996).
 - [11] R. Mettin, I. Akhatov, U. Parlitz, C. D. Ohl, and W. Lauterborn, Phys. Rev. E **56**, 2924 (1997).
 - [12] A. A. Doinikov, Phys. Rev. E **59**, 3016 (1999).
 - [13] A. Harkin, T. J. Kaper, and A. Nadim, J. Fluid Mech. **445**, 377 (2001).
 - [14] A. A. Doinikov, Phys. Rev. E **64**, 026301 (2001).
 - [15] Strictly speaking, the natural frequency is different from the resonance frequency. Because these frequencies are almost equal to each other in many cases, however, we treat them as the same, as has been done frequently.
 - [16] M. Ida, Phys. Lett. A **297**, 210 (2002).
 - [17] C. Feuillade, J. Acoust. Soc. Am. **98**, 1178 (1995).
 - [18] A. Prosperetti, Ultrasonics **22**, 69 (1984).
 - [19] This is not true when the driving pressure is strong. See, e.g., I. Akhatov, R. Mettin, C. D. Ohl, U. Parlitz, and W. Lauterborn, Phys. Rev. E **55**, 3747 (1997).
 - [20] M. Ida, J. Phys. Soc. Japan **71**, 1214 (2002).
 - [21] In this case, "in-phase", for example, means that during the sound pressure is *positive*, the bubble's radius is smaller than its equilibrium size and hence the deviation of the bubble's internal pressure is *positive*.
 - [22] L. A. Crum and A. I. Eller, J. Acoust. Soc. Am. **48**, 181 (1969).
 - [23] M. Ida, e-print, physics/0111138 (still in preparation).
 - [24] M. Ida, Comput. Phys. Commun. **150**, 300 (2003).
 - [25] M. Ida, Comput. Phys. Commun. **132**, 44 (2000).